Enhanced interpreter-aided salt-boundary extraction using shape deformation

Yang Zhang and Adam D. Halpert

ABSTRACT

In many marine seismic exploration projects, precise interpretation of the salt-body geometry (which is also called salt-body segmentation) is a key component of building the subsurface velocity model. However, segmentation of salt is very human-intensive, even with the help of currently available semi-automatic computer software. This paper addresses the problem of automatically and accurately tracking the salt boundary in a series of neighboring seismic image slices, given an accurate salt segmentation for only one single reference slice. (The reference segmentation can be done manually). We achieve this using a landmark-based shape deformation technique plus SVM (Support Vector Machine) style regression. An example on a 3-D Gulf of Mexico data set demonstrates the effectiveness of our approach.

INTRODUCTION

Interpreting the salt body in seismic images is of great importance for accurate velocity model building. Due to the poor quality of many seismic images, simple image processing filters followed by local boundary tracking algorithms give very poor results or fail easily. For example, in Figure 1, some parts of the salt boundary are simply missing from the image. A human interpreter's input is essential in these troublesome regions (Halpert et al., 2011). In the near term, the development of a super-algorithm that can fully automate boundary extraction without sacrificing the quality of the results is highly unlikely.

However, as today's seismic imaging practices evolve to three dimensions, manual interpretation of every single slice in a 3-D image cube is increasingly unrealistic. How can we achieve a good trade-off between the amount of manpower required and the quality of the boundary extraction result? The idea of manually segmenting only a small number of "key" slices and then intelligently propagating these results to the entire volume becomes attractive. Here we use a landmark-based shape-deformation technique to propagate a manual segmentation result of a single slice onto its neighboring slices, thus yielding a much better segmentation result overall than what we can achieve by simply applying fully automatic methods. The design goal for such intelligent boundary propagation consists of two parts:

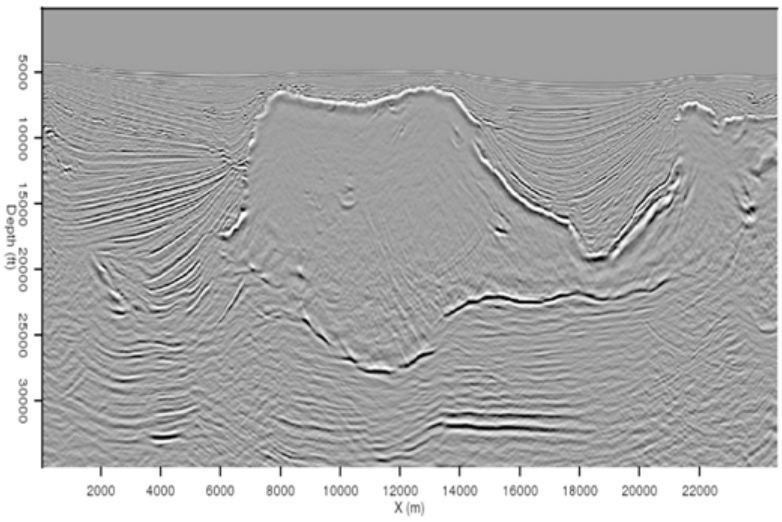

(a)

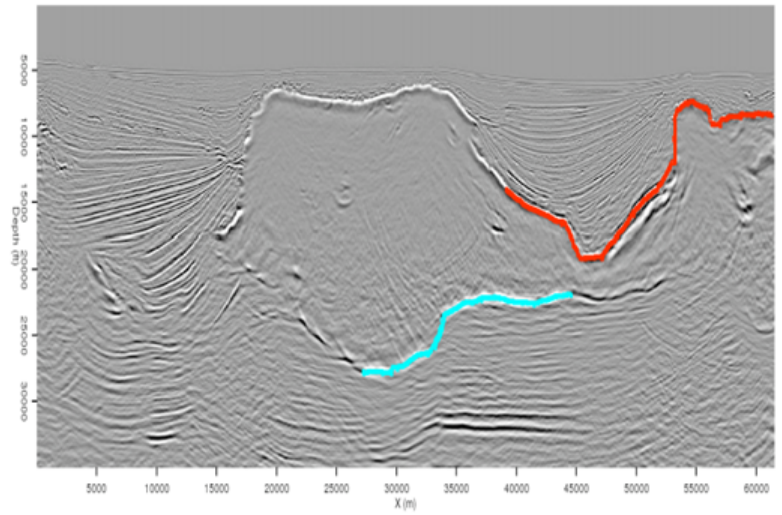

(b)

Figure 1: (a) A typical seismic image showing the salt body in the center. Some parts of the boundary are not well imaged due to the limited image quality. (b) The same image shown with the human-interpreted boundary. [**ER**]

- First of all, we force the new boundary to honor the available boundary information that can be confidently extracted from the image.
- Secondly, the new boundary should preserve the shape information known from the manual segmentation input, such that the boundary will deform reasonably where we do not have well-defined boundaries.

METHOD

Our approach is mainly based on the idea of Wang et al. (2001), described briefly here. Let us define the reference image slice that has been properly segmented as the *template image*, and define the image to which we want to propagate the segmentation result as the *input image*. The segmentation result in the template image is characterized by a set of contours. For simplicity, we assume that the template image contains only a single closed contour. Nonetheless, the extension of this method to handle multiple contours is straightforward.

We represent the known contour on the template image as a set of landmark points, $V = v_1, v_2, ..., v_n$ where $v_i = (x_i, y_i)$ (in 2-D Cartesian coordinates). Wang et al. (2001) describe the skeleton of this algorithm as follows:

> "For each landmark v_i, the proposed method first identifies a set of possible corresponding landmark points $B_i = \{v_i^{(j)}, j = 1, 2, ..., n_i\}$ on the input image, where $v_i^{(j)} = (x_i^{(j)}, y_i^{(j)})$. Then conceptually the deformation is solved in two major steps:
>
> 1. Identify the best landmark point v_i' from the landmark set B_i such that $V' = \{v_1', v_2', ..., v_n'\}$ is located in or near the true object boundary in the input image.
> 2. Deform the prior shape V to match V' while keeping the general shape characteristics of V. "

The cartoon in Figure 2 illustrates the idea of landmark-based contour deformation.

For the first step, we search the candidate points in set B_i along a short line segment that centers around point v_i and aligns to the contours normal direction $\mathbf{n_i}$. It is difficult to determine the best landmark point v_i' from all candidates in B_i at the first try. Therefore, we just choose randomly an element in each B_i to form the initial set V' and iterate this selection process a few times. During each iteration, we update the set V' such that V' more likely contains the correct corresponding landmarks.

The next deformation step is formulated by finding the optimal solution to an objective function which takes into account both the goal of deforming the points in V into the current landmark set V' and the goal of preserving the prior shape V

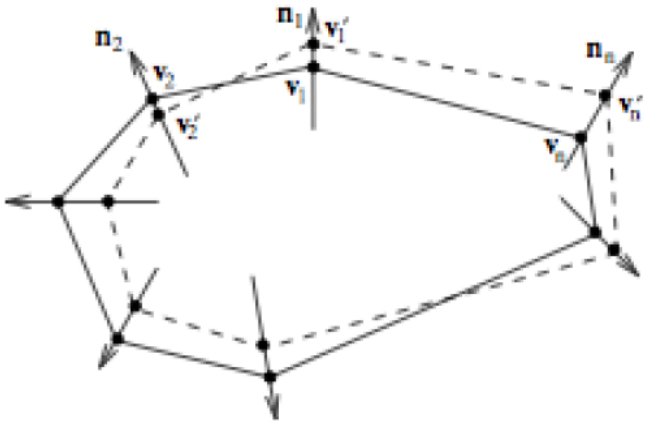

Figure 2: Landmark-based shape deformation, from Wang et al. (2001). [**NR**]

(using the bending-energy formula from (Bookstein, 1989)). The optimization goal is

$$\min_{V',\mathbf{t}} \left\{ \frac{1}{n} \sum_{i=1} Q(v_i', \mathbf{t}(v_i)) + \lambda \phi(\mathbf{t}) \right\} \tag{1}$$

in which $\mathbf{t}$ defines the deformation from V to V' as a mapping; i.e. $\mathbf{t} : (x, y) \rightarrow (f(x, y), g(x, y)) = (x', y')$. Function Q describes the term that penalizes the mismatch between V' (the landmarks we found on the input image) and the mapping defined by $\mathbf{t}(V)$. The Q term corresponds to the first goal, deforming the landmarks in set V to those in V'. Function $\phi(\mathbf{t})$ is a regularization term that tries to force the mapping $\mathbf{t}$ to be smooth, in other words, preserving the global shape information of the original V. We add a λ parameter to balance the weights of the two terms, Q and ϕ. The choice of λ is up to the user's judgment. After mathematical simplification, this optimization can be solved easily using the classical SVM(Support Vector Machine) regression technique (as a quadratic programming problem of size n). Moreover, the badly fitted components in set V' are identified as the support-vectors. We update the set V' by replacing those support-vectors with other candidates in B_i, such that the new set V' would achieve better fitting.

MATHEMATICAL SIMPLIFICATION

In this section, we reveal more mathematical details of this approach. The actual form of function Q in the objective function 1 is the ϵ-insensitive L1 norm:

$$||v_i' - \mathbf{t}(v_i)||_\epsilon = \begin{cases} 0, & \text{if } |v_i' - \mathbf{t}(v_i)| < \epsilon \\ |v_i' - \mathbf{t}(v_i)| - \epsilon, & \text{otherwise} \end{cases} \tag{2}$$

Since new landmark candidates in V' are sought along the contours normal direction $\mathbf{n_i}$, we constrain the desired mapping $\mathbf{t}(V)$ to displace v_i along direction $\mathbf{n_i}$ as well:

$$\mathbf{t}(v_i) = v_i + \gamma_i \mathbf{n_i}. \tag{3}$$

Let $\gamma = \gamma_i : i = 1, ..., n$. Since points in V' are found along the normal directions of the original contour V as well, we have $v'_i = v_i + h_i \mathbf{n_i}$. Then the previous problem 1 becomes

$$\min_{\mathbf{t},\gamma} \left\{ \frac{1}{n} ||h_i - \gamma_i||_\epsilon + \lambda \phi(\mathbf{t}) \right\}, \tag{4}$$

subject to constraint 3. As for, we choose the so-called bending-energy term, defined as

$$\phi(\mathbf{t}) = \int \int_{-\infty}^{+\infty} (E(f) + E(g))\, dxdy,$$

where

$$E(\bullet) = \left(\frac{\partial^2}{\partial x^2} \right)^2 + \left(\frac{\partial^2}{\partial y^2} \right)^2 + \left(\frac{\partial^2}{\partial x \partial y} \right)^2.$$

The nice thing about this choice of bending-energy is that we know in advance, given all mappings that satisfy constraint 3, the mapping specified by thin-plate spline interpolation will minimize the bending-energy (Bookstein, 1989). In other words, the solution $\mathbf{t}^*$ to the optimization problem 4 must be the thin-plate spline interpolation that maps $\{V : v_i, i = 1, ..., n\}$ to $\{\mathbf{t}(V) : \mathbf{t}(v_i) = v_i + \gamma_i \mathbf{n_i}, i = 1, ..., n\}$. Given that $\mathbf{t}$ must be a thin-plate spline interpolation, we can express $\phi(t)$ with the vector γ. Therefore, this variational problem (where the optimization parameters are functions not numbers) turns into a much simpler numerical convex optimization problem. We just need to find the optimal γ for the problem below:

$$\min_{\gamma} \left\{ \frac{1}{n} ||h_i - \gamma_i||_\epsilon + \frac{\lambda}{8\pi} (\hat{x}^T L \hat{x} + \hat{y}^T L \hat{y}) \right\}, \tag{5}$$

where $\hat{x}, \hat{y}$ is the vector representation of the x and y coordinates of the points in set $\mathbf{t}(V)$, and L is a semi-positive definite matrix defined by known quantities.

Using the standard SVM technique, we can instead solve the dual problem of 5 according to the K.K.T.(Karush–Kuhn–Tucker) conditions. It ends up being a standard quadratic programming problem with both upper and lower bounds.

EXAMPLES

We test this algorithm on a 3-D seismic image cube from a Gulf of Mexico seismic survey. The cube is of discrete size $970 \times 784 \times 12$ in the depth(Z), inline(X) and cross-line(Y) directions respectively. The grid spacings are 9.6 m, 25 m and 30 m. We test this algorithm on a 3-D seismic image cube from a Gulf of Mexico seismic survey. The cube is of discrete size $970 \times 784 \times 12$ in the depth(Z), inline(X) and cross-line(Y) directions respectively. The grid spacings are 9.6 m, 25 m and 30 m. We have only the human-interpreted segmentation result in slice 1, which we use as the template image. We then perform initial processing on this segmentation result to extract the template landmarks as shown in Figure 3.

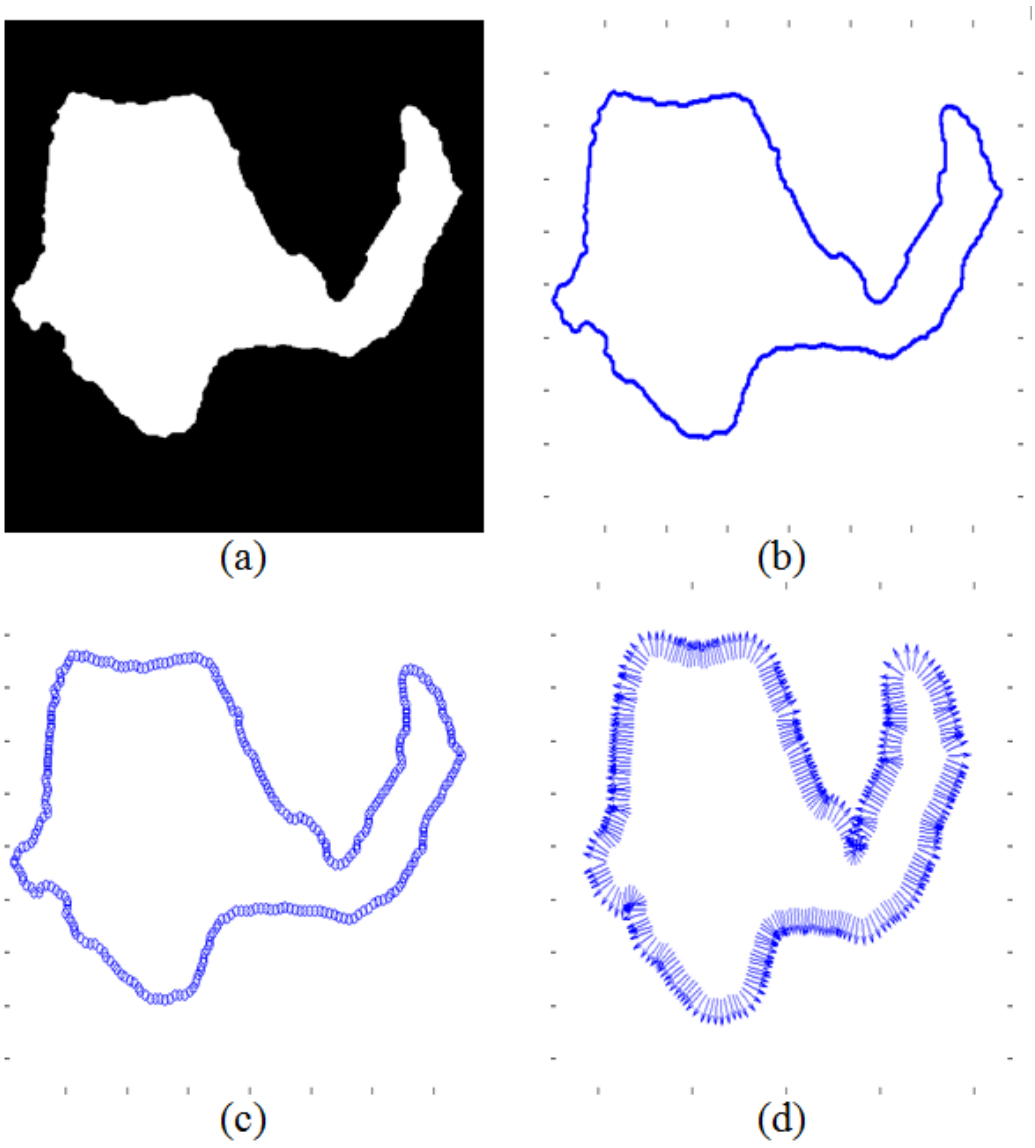

Figure 3: Preprocessing flow on the segmentation result of the template image. (a) Build the salt-body mask. (b) Extract the boundary. (c) Subsample to a list of landmarks. (d) The outnormal directions found for each landmark on the contour. [**CR**]

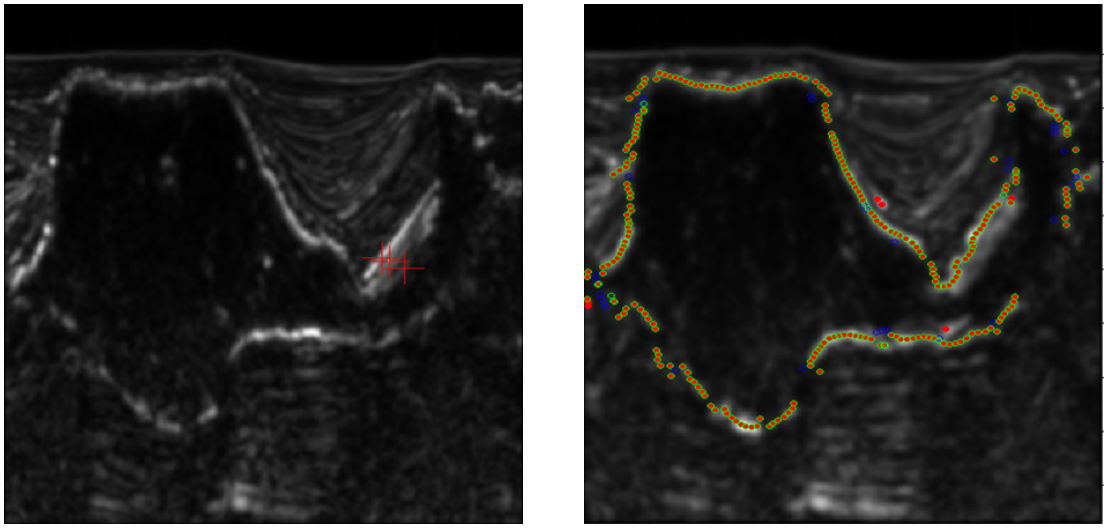

(a) (b)

Figure 4: a) The three candidate points found in B_{137}. b) The update of set V' in one iteration. Blue indicates points in V' that are support vector points, red shows the original points in V', and green shows the updated set V' obtained by replacing the badly fitting points in v'_i with better fitting candidates in B_i. [**CR**]

To find candidates for the set B_i, we overlay the landmark on the energy envelope of the input image (neighboring slice), then we search along the normal direction for certain image features which might suggest that certain locations be part of the boundary. Here we just use a very simple criterion: we choose the locations of the local amplitude maxima as the boundary point candidates. The plot in Figure 4(a) shows all candidates in B_i for $i = 137$.

We then run the optimization for a few iterations. During each iteration, we identify all the support vectors (which correspond to the fitting outliers); for each support vector h_i, we try to use other candidates in set B_i such that the fitting $h_i - \gamma_i$ improves. Figure 4(b) demonstrates this step during one iteration.

Finally we deform all 12 slices one by one, in increasing distance from the template slice. In Figure 5, we show the comparison between the obtained deformed boundary and the boundary found by automatic methods with the simple way of propagating the user input as described in Halpert et al. (2011). The improvement is prominent, with several regions highlighted in circles. The deformed boundary is less jagged and tracks the local edges in the image better. The shape-preserving constraint helps prevent boundary leakage as the automatic segmentation is done using flooding algorithms.

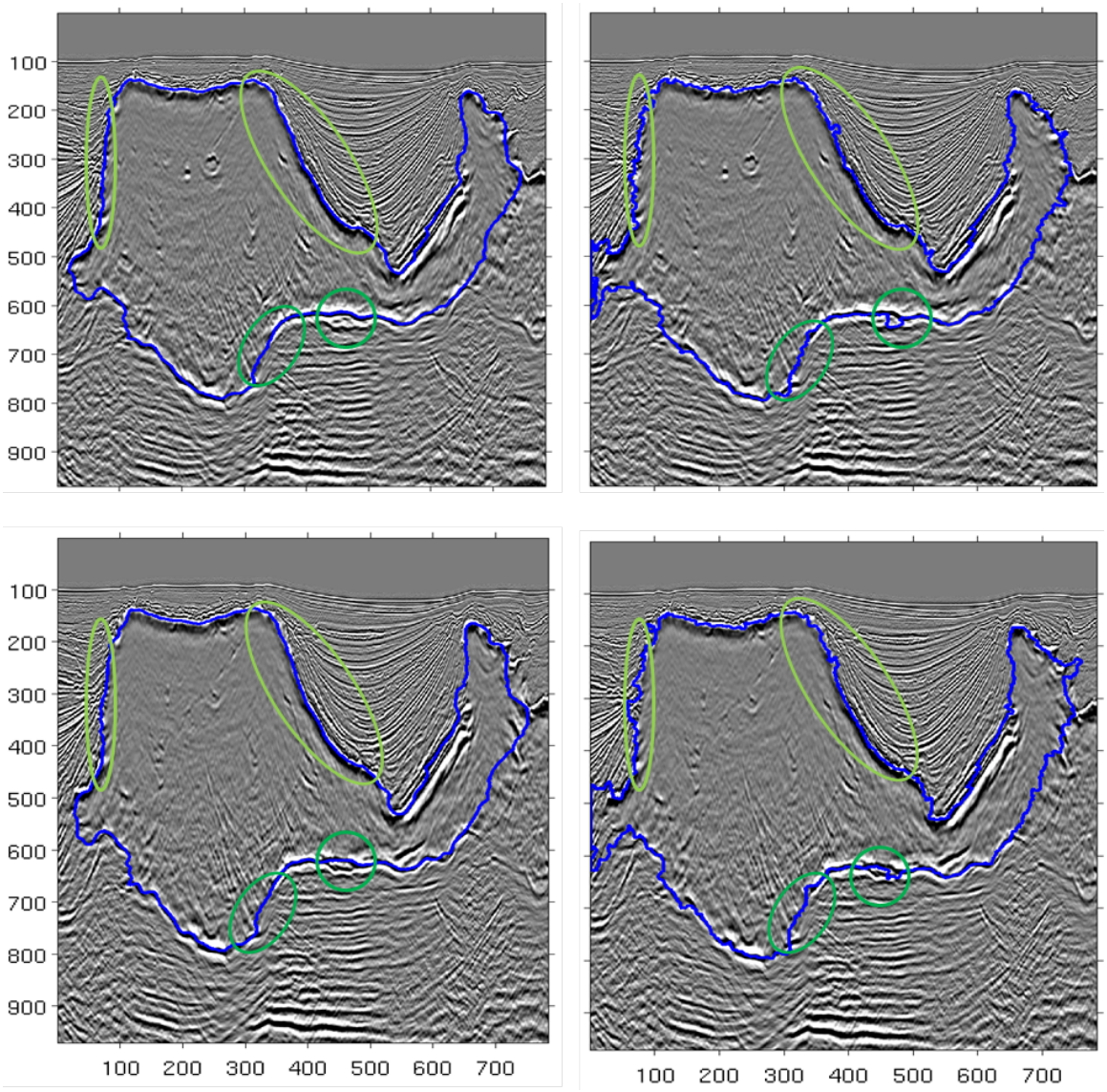

Figure 5: The segmentation result for slices 4 (top) and 12 (bottom) using our boundary deformation technique (left column) and the simple automatic method (right column). [**CR**]

CONCLUSION

In this paper, we improve salt-body segmentation for 3-D seismic images by deforming the accurate boundary on a human-interpreted slice into the neighboring slices. The deformation not only honors the available boundary information on the input slice, but also preserves the shape information from the template slice. Field data examples show very promising results. Possible additional applications of this method include the seismic tomography problem, where horizon-picking needs to be done for each of several non-linear iterations; meanwhile, the seismic image changes only slightly at each iteration.

ACKNOWLEDGMENTS

We thank WesternGeco for the seismic image used in this paper.

REFERENCES

Bookstein, F., 1989, Principal warps: Thin-plate splines and the decomposition of deformations: IEEE Trans. PAMI.

Halpert, A., R. Clapp, and B. Biondi, 2011, Interpreter guidance for automated seismic image segmentation: Presented at the Expanded Abstracts, EAGE 74th Annual International Conference and Exhibition.

Wang, S., W. Zhu, and Z.-P. Liang, 2001, Shape deformation: SVM regression and application to medical image segmentation: Proceedings on Eighth IEEE International Conference on Computer Vision, 209–216, IEEE.